RSC Advances

PAPER

View Article Online
View Journal | View Issue

Cite this: *RSC Adv.*, 2020, **10**, 37820

Cadmium sulfide net framework nanoparticles for photo-catalyzed cell redox†

Zhaoyu Chang,‡ Jian Zhang,‡ Wanyuan Dong, Xiangqi Meng, Hualei Wang, Dongzhi Wei and Yuhong Ren*

Received 22nd July 2020
Accepted 7th October 2020

DOI: 10.1039/d0ra08235j

rsc.li/rsc-advances

A strategy for synthesizing cadmium sulfide net framework (CdS-NF) nanoparticles was developed in a water-based system under mild reaction conditions. The CdS-NFs have not only the excellent photocatalytic properties of CdS, but also the large surface area and diverse porous structures of a metal–organic framework. An *Escherichia coli*–CdS-NF hybrid system was constructed using NADH regeneration to promote the conversion of trimethylpyruvate acid to L-*tert*-leucine. The *E. coli*–CdS-NF system showed higher NAD^+ recycling efficiency and substrate conversion rate than CdS QDs under visible light illumination. This work demonstrates a novel method for developing a brilliant coenzyme recycling photocatalyst in bio-redox reactions.

1. Introduction

Oxidoreductase plays an important role in the redox reaction. It catalyzes the reaction with cofactors for hydrogen sources and energy such as nicotinamide adenine dinucleotide (NADH) and its phosphorylated form (NADPH). However, cofactors are expensive and difficult to use in large-scale production.[1,2] Based on this situation, many researchers have focused on the regeneration of cofactors. The regeneration methods have been divided into six types.[3] Among them, photocatalytic regeneration has attracted increasing interest from researchers because the amount of solar energy is endless and half of the total sunlight is in the visible range.[4–6]

NAD^+ requires one proton and two electrons to regenerate NADH. Some semiconductors absorb solar energy to transfer protons and electrons with small bandgaps.[7] Three kinds of electron donors were often selected including triethanolamine[8] (TEOA), 2-[4-(2-hydroxyethyl)piperazin-1-yl]ethanesulfonic acid[9] (HEPES), and ascorbic acid (VC). Cadmium sulphide (CdS) has attracted the attention of researchers not only for its outstanding semiconductor optical and electrical properties but also for its suitable spectral absorption range.[10,11] The bandgap of CdS is 2.4 eV, and it can absorb visible light when semiconductor has a narrow band gap (E_g < 3.0 eV).[12] CdS nanoparticles have been used in many regions such as photocatalytic hydrogen production, solar batteries, and redox reactions.[13–15] In recent years, many different forms of CdS have been reported. Octadecene was used as a non-coordinating solvent for the synthesis of high-quality CdS nanocrystals.[16] CdS quantum dots (CdS QDs) were synthesized at high temperature to regenerate NADH.[17]

MOFs, also known as porous coordination polymers, are composed of metal ions or clusters as well as organic ligands through coordination bonds. MOFs have many special characteristics such as diverse porous structures, large surface areas and excellent mechanical stability.[18] Conventional nanocrystals cannot be fine-tuned and crystallized, thus exhibit inhomogeneity and long-range order from the atomic to micron scale regime that result in low protein loading efficiency and unstability.[19] Compared with traditional semiconductors, MOFs are considered promising candidates for cell catalysis applications. The zeolitic imidazolate framework-8 (ZIF-8) is a representative MOF formed by coordination between Zn^{2+} and 2-methylimidazole (2-MI).[20]

In this study, CdS was selected to transfer electrons to coenzyme NAD^+ to regenerate NADH. An efficient coenzyme self-circulation reaction was formed to promote the progression of the biocatalytic reaction. To improve the efficiency of the semiconductor-catalyzed redox reactions, we synthesized CdS net frameworks (CdS-NFs) *via* MOFs. Herein, Cd^{2+} was used to replace Zn^{2+} in composite MOF-$CdCl_2$ for the first time and sodium sulfide was then added to produce a CdS net framework structure. CdS is dispersed in the net framework, which is beneficial to transfer electrons to the cell redox reaction.

State Key Laboratory of Bioreactor Engineering, New World Institute of Biotechnology, East China University of Science and Technology, Shanghai 200237, China. E-mail: yhren@ecust.edu.cn; Fax: +86 21 6425 0068; Tel: +86 21 6425 2163

† Electronic supplementary information (ESI) available: Experimental details, Fig. S1–S3. See DOI: 10.1039/d0ra08235j

‡ These authors contributed equally to this work.

2. Experimental section

2.1 Materials and reagents

The plasmid pET28a-LDH was previously constructed in our laboratory. Cadmium chloride, sodium sulfide and ammonium

chloride were purchased from Yonghua Chemical Co., Ltd. (Shanghai, China). Trimethylpyruvate acid, 2-methylimidazole, and polyvinylpyrrolidone were purchased from Sigma-Aldrich (Shanghai, China). All other chemicals were purchased from Adamas-beta (Shanghai, China).

2.2 Synthesis method of CdS-NFs

The 10 mM cadmium chloride ($CdCl_2 \cdot 2.5H_2O$) dissolved in 50% ethanol was added to a round bottom flask. 2-Methylimidazole (2-MI) and polyvinylpyrrolidone polymer (PVP, $M_w = 40\,000$)[21] were dissolved in 50% ethanol and added into the flask with a constant pressure separatory funnel to control the dropping rate at 5–10 drops per second. Agitation and sonication were used to accelerate the reaction. In this case, the Cd^{2+}/2-MI ratio and the concentration of PVP were 1 : 4 and 2 wt%. After 20 min of reaction, the reaction solution was centrifuged (8000 × *g*, 10 min) and the precipitation was washed three times with pure ethanol and ultra-pure water. The precipitation was redissolved with 50% ethanol and added to a round bottom flask. The 10 mM Na_2S was added dropwise using a constant pressure separatory funnel. The bright yellow precipitation was observed obviously after reaction for 20 min. The reaction mixture was centrifuged (6000 × *g*, 10 min). The precipitation was washed three times with pure ethanol and pure water, and then freeze-dried for subsequent experiment. All reactions were performed at room temperature. The Cd^{2+}/2-MI ratio could be adjusted to 1 : 2, 1 : 4 and 1 : 8. The CdS-NF precipitation formed with Cd^{2+}/2-MI = 1 : 4 was washed with pure ethanol and pure water three times. After centrifugation, the supernatant was found to be bright yellow when the pellet was washed with water. The supernatant was placed in a 50 mL centrifuge tube at room temperature for a period of time, and then the CdS-NF solution was aggregated to form the precipitation.

2.3 Synthesis method of CdS quantum dots

The CdS QDs were synthesized in aqueous solution. The $CdCl_2 \cdot 2.5H_2O$ (10 mM) and thiourea (10 mM) were added to a 250 mL round bottom-flask, heated at 150 °C and stirred for 3 min to make them evenly mixed. $Na_2S \cdot 9H_2O$ (10 mM) was added to the reaction solution rapidly, and the mixing system continued with stirring and cooling at 100 °C at the same time. After reacting for 10 min, the solution was cooled to room temperature. The solution was centrifuged (7500 × *g*, 10 min) and the precipitation washed three times with pure ethanol and pure water.

2.4 *Escherichia coli* expression

Leucine dehydrogenase from *Labrenzia aggregate* was constructed in pET-28a and then transformed into *Escherichia coli* BL21 (DE3). The strain was cultured in 200 mL Luria broth (LB) at 37 °C. The 1 M isopropyl β-D-1-thiogalactopyranoside (IPTG) was added to flask when the optical density at 600 nm (OD_{600}) reached 0.6, and the protein expression was induced at 18 °C for 20 h. The cell cultures were collected by centrifugation at 7500 × *g* for 10 min, and then the cell pellet was freeze-dried.

2.5 Aggregation of cell-CdS

Three different CdS were weighed in a beaker and dissolved with 2 mL pure water to the concentration of 3 g L^{-1} and then sonicated for 15 min. The lyophilized resting cells were added to the beaker and the ratio of CdS to cells was set to 3 : 1. The mixed solution was then agitated for 1 hour at 4 °C and the aggregates were collected by centrifugation at 7500 × *g* for 10 min. The cell-CdS aggregates were washed with pure water for three times.

2.6 Characterizations

To characterize and optimize the synthesized CdS nanoparticles, multi-angle laser light scattering (MALS) was carried out on a Wyatt GPC/SEC (America). The samples were diluted to 1 g L^{-1}. The XRD experiments were performed on a Rotating Anode X-ray Powder Diffractometer with model i18KW/D/max2550VB/PC operating at 40 kV and 100 mA. The patterns were collected over a 2θ range from 5° to 75° with a scanning speed of 12° min^{-1}. Nitrogen adsorption and desorption isotherms were performed on an ASAP 2020 analyzer (Micromeritics, USA) at 77 K after samples degassed under a vaccum of 623 K for 6 h. The total pore volumes were determined under the condition of $p/p_0 = 0.99$. The Brunauer–Emmett–Teller (BET) method was used to determine the surface areas and the pore volumes.

Three kinds of CdS nanoparticles were characterized by field-emission scanning electron microscopy (FE-SEM). Nanoparticles were dissolved in ethanol and dispersed by sonication for 10 min, and then added (10 μL) to a silicon wafer and dried at room temperature. The field-emission scanning electron microscopy images were observed on Gemini 500 SEM (Germany). In addition, the crystal lattice of CdS in CdS-NF was characterized by high-resolution transmission electron for JEM 2100 (Japan). To characterize the cell-CdS aggregates, transmission electron microscopy (TEM) was used to observe the binding of cells to nanoparticles. The aggregated samples were resuspended with pure water, and 10 μL suspension was added to a copper mesh dried at room temperature. The images were characterized by JEM 1400 (Japan).

2.7 Optimization of photocatalytic conditions and detection of trimethylpyruvate acid by HPLC

A 3 mL transparent vial was subjected to photocatalysis in water bath at 30 °C under 460 nm light. The photocatalytic reaction system contained 200 mM HEPES (pH = 8.0), 200 mM ammonium chloride, 1 g L^{-1} cells, 10 mM trimethylpyruvate acid, electron donor, and photocatalyst under 460 nm LED light. After reacting for 72 h in a 30 °C water bath, 300 μL aliquots were taken every 12 h and centrifuged at 13 000 × *g* for 7 min. The substrate sample liquid analysis method has been reported.[22]

The electron donor sacrifices electrons to the photocatalyst to avoid recombining electrons and holes. The effect of different electron donors on the photocatalytic reactions was determined by three different electron donors, including 200 mM HEPES,

150 mM TEOA, and 200 mM VC. The reaction was performed for 72 h under 460 nm LED illumination.

The conversion of trimethylpyruvate acid to L-*tert*-leucine requires reducing force provided by NADH cofactor. The substrate was catalysed in water bath at 30 °C for 72 h and the conversion efficiency was measured by HPLC to determine the effect of exogenous 0.5 mM NADH and 1 g L^{-1} cells containing cofactors on the photocatalytic reaction. The effect of photocatalyst concentration on the photocatalytic reaction was determined by setting CdS-NF concentration gradients (2, 5, and 10 mM) to analyse the substrate conversion rate. The influence of LED illumination on the photocatalytic reaction was determined by 460 nm LED light illuminate reaction for 72 h, and dark condition was used as a control group. The effect of light intensity on photocatalytic reaction was determined by setting the light intensity gradients (1.86, 2.29, and 3.77 mW cm^{-2}) to measure the substrate conversion rate.

3. Results and discussion

3.1 CdS nanoparticles assay

In this reaction system, cadmium chloride was dissolved in ethanol which used as the triggered solvent; 2-methylimidazole (2-MI) and polyvinylpyrrolidone polymer (PVP, M_w = 40 000) were served as stabilizers and added to the mixed solution with agitation and ultra-sonication. After 20 min of mixing, white precipitation was appeared and then collected by centrifugation at 7500 × *g* for 10 min. The precipitation was washed with pure ethanol and ultra-pure water to obtain MOF-$CdCl_2$ (Fig. 1A). Sodium sulfide was added to the reaction system after dissolving MOF-$CdCl_2$ with ethanol. As the reaction proceeded, bright yellow precipitation was appeared in the reaction vessel and identified as CdS-NFs (Fig. 1A).

The synthesis conditions of CdS-NFs including the reaction solution and the ratio of Cd^{2+}/2-MI were optimized in this study. The size of CdS-NFs was characterized by Wyatt GPC/SEC-MALS. CdS-NFs synthesized in ethanol had small particles (~10 nm; Fig. S1†). For comparison, the molar ratio of Cd^{2+}/2-MI in the ethanol system was changed to obtain different sizes of products. Cd^{2+}/2-MI = 1 : 2 and 1 : 4 were set in this experiment. The yield of the precipitation at Cd^{2+}/2-MI = 1 : 4 (23.4%) was greater than Cd^{2+}/2-MI = 1 : 2 (18.3%). However, the particle distribution was similar in both systems, ranging from 1 nm to 100 nm (Fig. S2†). We further compared the particle size of MOF-$CdCl_2$ and CdS-NFs. The particle size of CdS-NFs was larger than MOF-$CdCl_2$ when sodium sulfide was added into the system (Fig. 1B and C).

The CdS-NF precipitation was washed with ultrapure water and then centrifuged. The supernatant was bright yellow, which indicated the formation of CdS-NF nanoparticles. After keeping at room temperature for a period of time, the bright yellow supernatant was aggregated to form precipitation.

To compare the photocatalysis efficiency of CdS-NFs with traditional CdS, CdS quantum dots (QDs) was introduced in this study. CdS QDs were synthesized under high temperature conditions, resulting in the formation of small particles of about 5 nm, but they were difficult to dissolve in water (Fig. 1D).

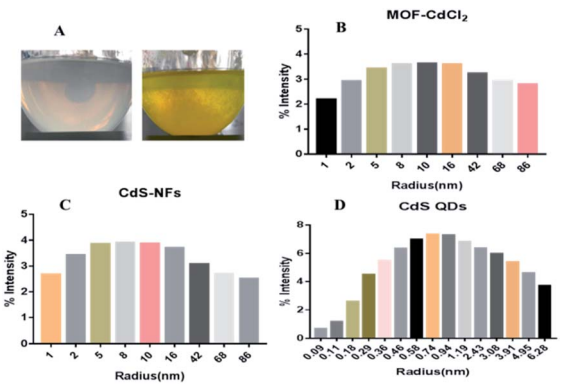

Fig. 1 (A) Precipitation of synthetic MOF-$CdCl_2$ and CdS-NFs. (B)–(D) CdS nanoparticles were characterized by Wyatt GPC/SEC-MALS.

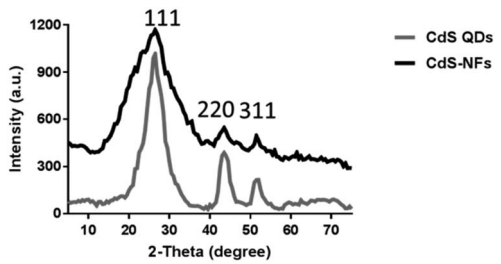

Fig. 2 X-ray diffraction spectrum of CdS QDs and CdS-NF nanoparticles.

3.2 X-ray diffraction

X-ray diffraction analysis of the CdS samples obtained from different synthesis methods revealed that CdS QDs and CdS-NF nanoparticles were corresponding with cubic lattice. The peak can be classified as the 111, 220, and 311 (PDF, file no. 10-0454). The crystallite sizes of CdS QDs and CdS-NFs were estimated to be 2.85 and 5.61 nm, according to the Scherrer equation (Fig. 2).[23]

The pattern of CdS samples showed that synthesis temperature had a great influence on the formation of nanocrystals. The diffraction peaks would be shaped and the crystallization would be better as the synthesis temperature rose. The CdS-NF nanoparticles were synthesized at room temperature and the peak was broadened. In addition, an amorphous state was formed with the addition of organic materials and polymers, which resulted in weaker peak intensity of CdS-NFs.

Table 1 Porous characteristic of CdS samples

Samples	BET surface area (m^2 g^{-1})	Pore volume (m^3 g^{-1})	Pore size (nm)
CdS QDs	158.90	0.27	7.3
CdS-NFs	142.79	0.41	20

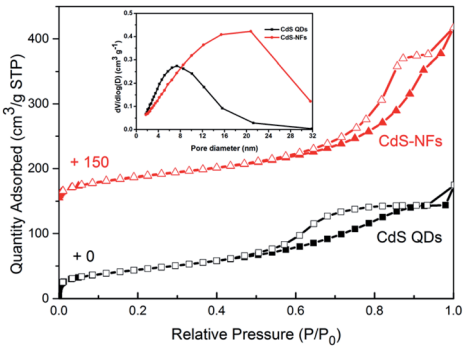

Fig. 3 N_2 adsorption (solid symbols) and desorption (open symbols) for CdS QDs and CdS-NFs. The inset image shows the mesopore size distribution.

3.3 Nitrogen adsorption and desorption curves

Nitrogen adsorption and desorption isotherms in Fig. 3 showed the textural characteristics of CdS QDs and CdS-NFs. The BET surface area, pore volume, and pore size were presented in Table 1. At very low particle pressure ($p/p_0 < 0.1$), the nitrogen physical adsorption of CdS QDs exhibited a steep absorption, which confirmed the presence of micropores.[24] CdS-NFs displayed a combination of type II isotherm and H_4 hysteresis loop, and were characterized by a relative pressure p/p_0 of 0.43. This type of hysteresis loop suggested that the CdS-NF nanoparticles contain mesopores.[25] CdS QDs nanoparticles are easy to aggregate and lead to the existence of hysteresis loop, which can be proved in the FE-SEM images of CdS QDs (Fig. 4D).

3.4 Electron microscope assay

The size and morphology of the precipitation and supernatant were characterized by field emission scanning electron microscope (FE-SEM) and high-resolution transmission electron microscope (HRTEM) (Fig. 4A, B and S3†). The images showed that the supernatant of CdS-NF formed a network and porous structures. CdS was combined with the network structure, and the particles size were about 5 nm (Fig. 1A and B). The FE-SEM image indicated that the precipitation was composed of two nanomaterials: one was CdS-NFs that formed the net framework, and the other was a shuttle structure of about 200 nm. The sediment was washed by ultra-pure water until CdS could not be detected in the supernatant. The precipitation was then characterized by FE-SEM and the results showed that the shuttle structure could not be found. There was only the network structure detected in precipitation (data not shown), which indicated that the shuttle-shaped materials were aggregates of CdS-NFs (CdS-NFs-A). Only shuttle-like aggregates without the CdS network structure were obtained when the ratio of Cd^{2+}/2-MI = 1 : 8 (Fig. 4C). The size of the CdS-NFs-A particles was more than 500 nm. The morphology of CdS QDs was characterized by FE-SEM in Fig. 4D. The size of the CdS QD particles was less than 5 nm. However, CdS QDs were aggregated easily and difficult to disperse.

Next, to demonstrate the photocatalytic performance of CdS-NF semiconductors, leucine dehydrogenase (LDH) from *Lab-renzia aggregate* was selected to combine with CdS-NFs through electrostatic interactions. Leucine dehydrogenase was constructed in *Escherichia coli* BL21 (DE3) and a cell-CdS hybrid system was developed. The hybrid system makes use of the CdS to transfer proton and electron to regenerate NADH in the conversion of trimethylpyruvate acid to L-*tert*-leucine.

The morphology of the cell-CdS-NF, cell-CdS-NFs-A and cell-CdS QD aggregates was observed by TEM (Fig. 5). CdS-NFs were bound to the cell *via* non-covalent interactions, and the combined areas increased because of the net framework structure (Fig. 5A). CdS-NFs and CdS-NFs-A were synthesized *via* organic substances, and the cell membrane is composed of lipid-soluble substances. We speculated that the organic matter

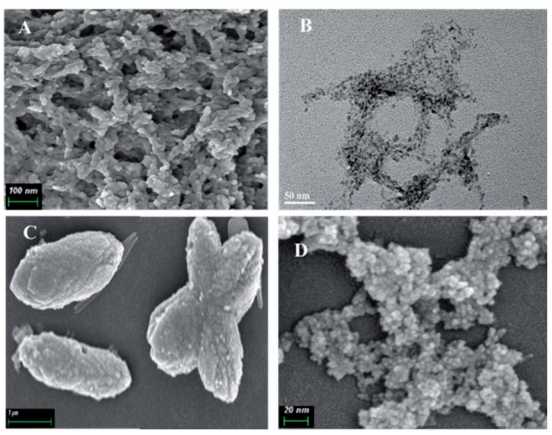

Fig. 4 CdS-NF, CdS-NFs-A, and CdS QDs were characterized by FE-SEM and TEM. (A) FE-SEM image of the supernatant of CdS-NF. Scale bar = 100 nm; (B) TEM image of the supernatant of CdS-NF; (C) FE-SEM image of the CdS-NFs-A formed with Cd^{2+}/2-MI = 1 : 8. Scale bar = 1 μm; (D) the morphology and size of CdS QDs particles were observed by FE-SEM. Scale bar = 20 nm.

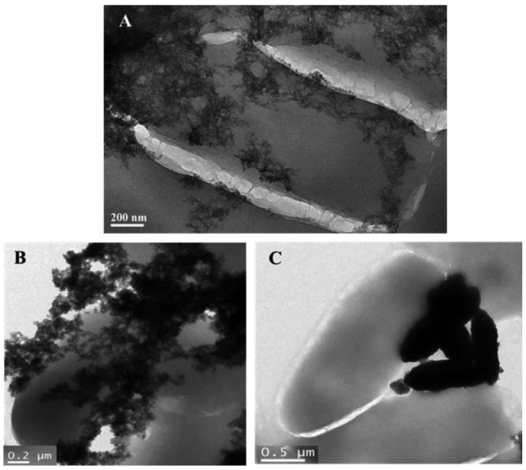

Fig. 5 TEM images showed the morphology of three nanoparticles combined with *Escherichia coli*. (A) The morphology of cell-CdS-NF aggregates observed by TEM. (B) The morphology of cell-CdS QD aggregates. Scale bar = 0.2 μm. (C) An image of cell-CdS-NFs-A aggregates. Scale bar = 0.5 μm.

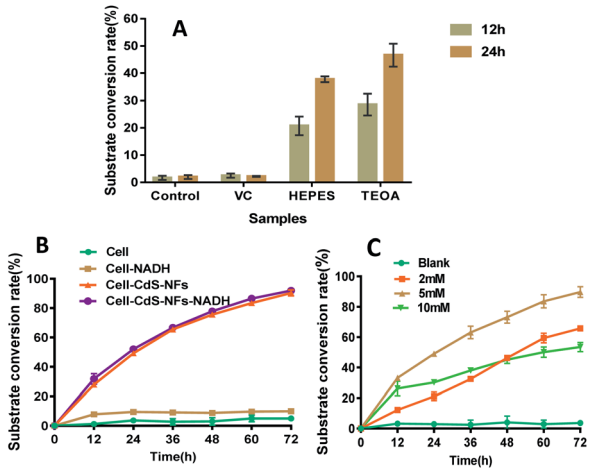

Fig. 6 Effect of electron donor, NADH, and photocatalyst concentration in photocatalysis reaction. (A) Effects of three electron donors on CdS photocatalysis; (B) the influence of NADH on photocatalysis; and (C) CdS-NF concentration affects photocatalytic efficiency.

contained in CdS-NFs has a high affinity with the fat-soluble cell membrane. The morphology of the cell-CdS QD aggregates changed from rod-shaped to spherical, which is due to the self-aggregation of CdS nanoparticles that bound to the cell surface (Fig. 5B). This phenomenon was not observed in the cell-CdS-NF and cell-CdS-NFs-A aggregates (Fig. 5C), which indicated that the network acted as surfactant to avoid CdS aggregation.

3.5 Effect of electron donor, NADH, and photocatalyst concentration on the efficiency of photocatalysis reaction

HEPES was used as the reaction buffer solution, and TEOA was the electron donor (Fig. 6A). Ascorbic acid was not suitable as an electron donor in this reaction system because the optimal pH of LDH is 8.5. The substrate conversion efficiency of the coenzyme contained in the cell was as high as 91% after 72 h of irradiation, which was similar to the addition of NADH (Fig. 6B). This result suggested that exogenous addition of 0.5 mM NADH did not participate in intracellular photocatalysis; therefore, the CdS-cell reaction system does not need exogenous NADH.

The influence of CdS-NF concentration and illumination intensity on photocatalysis was studied. Only 6.5 mM trimethylpyruvate acid reacted after 72 h of illumination when 2 mM CdS-NFs were added to the hybrid system (Fig. 6C). To improve the efficiency of the reaction, a longer reaction time was required in this experiment. When the CdS-NF concentration increased to 10 mM, the substrate consumption rate was as high as 30% within 12 h, which is similar to the result of 5 mM CdS-NF photocatalysis. However, the substrate conversion rate curve gradually became smooth as the reaction progressed. We suspected that high concentration of CdS-NFs would be toxic to cells. Therefore, 5 mM CdS-NFs were selected for photocatalysis.

3.6 Effect of LED illumination, and light intensity in photocatalysis reaction

The substrate conversion rate of CdS-NF photocatalysis was only 10% in the absence of 460 nm LED illumination, which is close to the control group that without CdS-NFs. The trimethylpyruvate acid conversion rate was as high as 95% at 72 h (Fig. 7A), and the photocatalytic efficiency was increased by 9.5-fold under the light. The efficiency of photocatalytic reactions is thus clearly dependent on illumination. Three types of photocatalytic reactions with different light intensities were studied. The substrate conversion rate was 93% under an illumination of 2.29 mW cm^{-2} and showed a 1.3-fold increase compared with 3.77 mW cm^{-2} light intensity. These indicated that the illumination intensity also affects CdS-NF photocatalysis (Fig. 7B). Therefore, the illumination intensity must be controlled in photocatalysis because high intensity light will destabilize the enzymes in the cell when the photocatalyst is present. An illumination intensity of 2.29 mW cm^{-2} was finally selected.

3.7 Efficiency of different CdS nanoparticles in photocatalytic reaction

Three kinds of CdS including CdS QDs, CdS-NFs-A and CdS-NFs were added to the hybrid photocatalytic reaction respectively. The results showed that the conversion rate of CdS-NF photocatalytic trimethylpyruvate acid was as high as 95% under optimal reaction conditions, and the cofactor-recycling

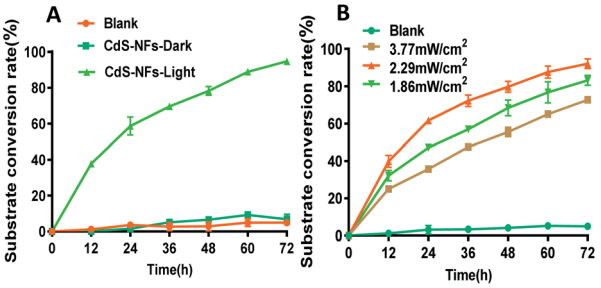

Fig. 7 Effect of LED illumination and light intensity in photocatalysis reaction. (A) Illumination condition affects photocatalysis; and (B) influence of illumination intensity on photocatalysis.

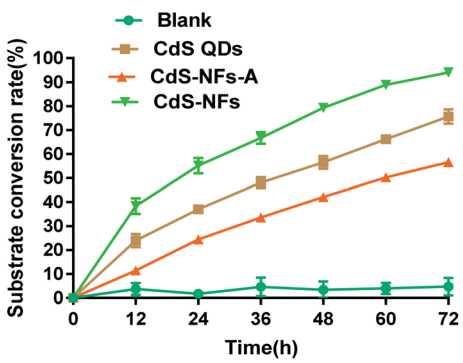

Fig. 8 The conversion rate of trimethylpyruvate acid that photocatalyzed by three different kinds of CdS. The reaction system includes 200 mM HEPES, 200 mM NH_4Cl, 150 mM TEOA, 10 mM trimethylpyruvate acid, 1 g L^{-1} resting cells, 5 mM photocatalyst, and a light intensity of 2.29 mW cm^{-2}. Blank represents the reaction system without photocatalyst.

frequency (TOF) increased by 19-fold *versus* blank (Fig. 8). The cofactor-recycling frequency (TOF) is defined as the total turnover number of NAD^+ per hour (TTn per h), in which TTn = [mol (product or substrate)][mol NAD^+]$^{-1}$.[22] However, the substrate conversion rate of CdS QD photocatalytic reaction was 70% and the TOF was increased by 14-fold. The photocatalytic efficiency of CdS-NFs-A was not satisfactory with a substrate conversion of only 55% and the TOF was increased by 11 times.

CdS-NF nanomaterials formed a large network and porous structure with CdS distributed on the network. Such a large surface area and high affinity contribute to the binding of CdS with cells, thereby improving the efficiency of electron transfer. The diameter of the CdS QD nanoparticles was less than 5 nm, but it tend to form large agglomerations that affected the efficiency of the photocatalytic reaction. In addition, the CdS QDs had weak affinity to cell membrane and just bound to the cell with electrostatic interactions. The CdS-NFs-A formed shuttle-shaped nanomaterials with a size over 500 nm, leading to a recombination of electrons and holes, which reducing the electron transfer efficiency.

4. Conclusions

In this study, we developed a novel method to synthesize CdS-NF nanoparticles in aqueous environment under ambient conditions. The CdS-NFs have not only the excellent photocatalytic properties of CdS, but also the large surface area and diverse porous structures of metal–organic framework. Compared with conventional CdS synthesis methods, this strategy is reliable, environmental friendly, and easier to implement. The solubility of cadmium sulphide was greatly improved in this reaction. In addition, CdS-NFs acted as the photocatalyst and covalently bound with *Escherichia coli* to catalyze the regeneration of cofactor, thereby promoting the conversion of trimethylpyruvate acid to L-*tert*-leucine. Furthermore, CdS-NFs have a higher photocatalytic efficiency than CdS QDs. In future, CdS-NFs will have broader prospects in the field of photocatalysis.

Conflicts of interest

The authors declare no conflict of interest.

Acknowledgements

This work was funded by the National Natural Science Foundation of China (No. 21778018), Natural Science Foundation of Shanghai (19ZR1412700), Fundamental Research Funds for the Central Universities (No. 222201814035) and Research Program of State Key Laboratory of Bioreactor Engineering.

References

1 F. Hollmann, I. W. C. E. Arends and D. Holtmann, *Green Chem.*, 2011, **13**, 2285–2314.
2 X. D. Wang and H. H. P. Yiu, *ACS Catal.*, 2016, **6**, 1880–1886.
3 X. D. Wang, T. Saba and H. H. P. Yiu, *Chem*, 2017, **2**, 621–654.
4 S. S. Bhoware, K. Y. Kim, J. A. Kim, Q. Wu and J. L. Kim, *J. Phys. Chem. C*, 2011, **115**, 2553–2557.
5 O. Diwald, T. L. Thopson, T. Zubkov, G. Goralski, W. S. D. Alck and J. T. Yates, *J. Phys. Chem. B*, 2004, **108**, 6004–6008.
6 J. L. Guo, M. Suástegui, K. K. Sakimoto, V. M. Moody and G. Xiao, *Science*, 2018, **362**, 813–816.
7 H. L. Huang, Y. Jina, Z. G. Chaia and X. R. Gu, *Appl. Catal., B*, 2019, **257**, 117869.
8 K. Kinastowska, J. Liu, J. M. Tobin and Y. Rakovich, *Appl. Catal., B*, 2019, **243**, 686–692.
9 K. A. Brown, D. F. Harris and M. B. Wilker, *Science*, 2016, **352**, 448–450.
10 F. Chen, R. Zhou, L. Yang, M. Shi, G. Wu, M. Wang and H. Chen, *J. Phys. Chem. C*, 2008, **112**, 13457–13462.
11 Y. Huang, F. Sun, T. Wu, Q. Wu, Z. Huang, H. Su and Z. Zhang, *J. Solid State Chem.*, 2011, **184**, 644.
12 M. R. Gholipour, C. T. Dinh, F. Beland and T. O. Do, *Nanoscale*, 2015, **7**, 8187–8203.
13 W. Wei, P. Q. Sun and Z. Li, *Sci. Adv.*, 2018, **4**, 9253–9260.
14 M. Mollavali, C. Falamaki and S. Rohani, *Int. J. Hydrogen Energy*, 2018, **43**(19), 9259–9278.
15 K. A. Brown, D. F. Harris and M. B. Wilker, *Science*, 2016, **352**, 447–451.
16 W. W. Yu and X. G. Peng, *Angew. Chem., Int. Ed.*, 2002, **41**, 2368–2371.
17 D. H. Nam, S. H. Lee and C. B. Park, *Small*, 2010, **6**, 922–926.
18 R. Zhai, Y. F. Yuan, F. L. Jiao, F. R. Hao and X. Fang, *Anal. Chim. Acta*, 2017, **994**, 19–28.
19 J. D. Cui, Y.-X. Feng, T. Lin, Z.-L. Tan, C. Zhong and S. Jia, *ACS Appl. Mater. Interfaces*, 2017, **9**, 10587–10594.
20 R. Banerjee, H. Furukawa, D. Britt, C. Knobler and O. M. Yaghi, *J. Am. Chem. Soc.*, 2009, **131**, 3875–3877.
21 F. K. Shieh, S. C. Wang, S. Y. Leo and K. C.-W. Wu, *Chem.–Eur. J.*, 2013, **19**, 11139–11142.
22 X. Gao, S. Yang, C. C. Zhao and Y. H. Ren, *Angew. Chem., Int. Ed.*, 2014, **53**, 14027–14030.
23 K. Matjaž, B. Irena and D. Anita, *Ultrason. Sonochem.*, 2010, **17**, 916–922.
24 D. L. Jin, G. H. Ye and J. W. Zheng, *ACS Catal.*, 2017, **7**, 5887–5902.
25 G. H. Ye, Y. Y. Sun, Z. Y. Guo and K. K. Zhu, *J. Catal.*, 2018, **360**, 152–159.